Journal of Constructional Steel Research 112 (2015) 1–9

Contents lists available at ScienceDirect

Journal of Constructional Steel Research

Flapwise bending vibration of rotating tapered Rayleigh cantilever beams

A.-Y. Tang [a,b], X.-F. Li [b,*], J.-X. Wu [b], K.Y. Lee [c,d]

[a] College of Town Resources and Planning Science, Jishou University, Zhangjiajie 427000, PR China
[b] School of Civil Engineering, Central South University, Changsha 410075, PR China
[c] State Key Laboratory of Structural Analysis for Industrial Equipment, Dalian University of Technology, Dalian 116024, PR China
[d] Department of Engineering Mechanics, Dalian University of Technology, Dalian 116024, PR China

ARTICLE INFO

Article history:
Received 24 September 2014
Accepted 17 April 2015
Available online xxxx

Keywords:
Rotating beam
Free vibration
Rayleigh beam theory
Rotary inertia
Natural frequency

ABSTRACT

Free vibration of rotating tapered cantilever beams with rotary inertia is studied.The cross-sectional area and its moment of inertia vary along the length. The governing differential equation of vibration of rotating Rayleigh beams is derived using Hamilton's principle, and the integral equation method is proposed to determine the natural frequencies. For rotating non-uniform beams with power-law varying width and height, numerical results of the natural frequencies are obtained for different taper ratios, angular velocities and hub radii. The solutions are validated by comparison with the results in open literature. The effects of the rotary inertia, angular velocity, taper ratio and hub radius are analyzed and presented in tables and graphs. Resonance is also analyzed.

1. Introduction

Rotating cantilever beams with varying cross-sections are widely used as structural elements in the engineering field. Many engineering components can be idealized as cantilever beams rotating around a fixed axis such as helicopter blades, aircraft propellers, turbine blades, and wind mill turbines. Study on free vibration of such rotating cantilever beams is of great significance for understanding mechanical behaviors and structural reliability of these components. Since rotating speed strongly affects the dynamic behavior of these structures, the variation of the natural frequencies closely depends on the rotating speeds as well as the geometry of cantilever beams. To achieve optimal performance of rotating cantilever beams, the dynamic behavior analysis has attracted considerable attention.

A lot of researches on free vibration analysis of rotating cantilever beams have been made for those with variable cross-sections. For rotating beams with linearly varying width and constant height, vibration has been studied based on the finite element method [1,2]. Another similar case of rotating beams with linearly varying height and constant width has been investigated in [2,3]. Also, rotating beams with linearly varying width and height were further studied [4–6]. In [7], a rotating beam having a linear mass variation and a fourth-order polynomial stiffness variation was considered for different taper ratio parameters. A more general case studied is a rotating beam with constant width and power-law varying height [8]. When the taper ratio vanishes, rotating uniform beams can be reduced from tapered beams [9,10]. An integral equation method has been proposed to treat free vibration of rotating non-uniform Euler-Bernoulli beams [11]. For a rotating inclined Euler beam at constant angular velocity, the finite element method was also used to determine the natural frequencies [12].

For rotating cantilevers, the existence of coupling effects in all directions makes the determination of natural frequencies complex. Rao and Gupta [13] evaluated the natural frequencies and mode shapes of bending–bending vibration in the flapwise and chordwise directions through the finite element technique. Free vibration analysis of a rotating, double tapered Timoshenko beam considering flapwise bending-torsion coupling was performed by Ozgumus and Kaya [5]. Furthermore, a rotating beam featuring bending–bending-torsion coupling was analyzed [14]. Besides, a vibration analysis considering stretching–bending coupling has been formulated by Yoo and Shin [15], who introduced gyroscopic coupling terms to give numerical natural frequencies. Based on a dynamic modeling method, Chung and Yoo [16] considered the stretch deformation for a rotating beam coupled with chordwise deformation, and uncoupled with the flapwise deformation. The flapwise bending vibration coupled with lagwise bending and axial vibration was investigated by Huang et al. [17]. The coupling between flapwise and chordwise bending vibration was considered by Zhu [18].

In addition, the dynamic analysis of a rotating non-uniform beam has been made based on various approaches including analytical and numerical ones. However, achieving an explicit solution is difficult since a set of partial differential equations with variable coefficients are encountered. For general situations, there exist few exact explicit solutions except certain special cases with the aid of special functions such as Bessel functions. So deriving approximate or numerical solutions becomes main stream, and a great number of methods have been devoted

* Corresponding author. Tel.: +86 731 8816 7070; fax: +86 731 8557 1736.
E-mail address: xfli@csu.edu.cn (X.-F. Li).

http://dx.doi.org/10.1016/j.jcsr.2015.04.010
0143-974X/

to this topic. One of the most representative schemes is to appeal to the finite element method (FEM). The dynamic behavior of a rotating Euler–Bernoulli beam has been analyzed based on the FEM [2,16]. When rotary inertia is taken into account, Ansary [19] applied the FEM to study the free vibration of rotating uniform beams. Wang and Wereley [10] adopted a slightly different FEM to deal with a low-degree-of-freedom model for dynamic analysis of rotating tapered beams. Differing from the FEM, the differential transformation method (DTM) as a semi-analytical method was used in [5,8,20] to study the vibration characteristics of a rotating tapered cantilever beam.

In addition to the FEM and DTM, other approaches have also been presented to handle free vibration of rotating beams. For example, the Frobenius method was suggested in [6,21–23] to formulate the dynamic stiffness matrix to cope with the dynamic analysis of a rotating uniform or tapered beam according to Euler–Bernoulli and Timoshenko theories of beams. The Rayleigh–Ritz method was used to study the vibration characteristics of a rotating beam [7,18]. The Wentzel, Kramers and Brillouin (WKB) approximation was employed by Firouz-Abadi et al. [4] to investigate the transverse free vibration of a class of variable-cross-section beams. In this approach, a solution of the governing equation of a rotating Euler–Bernoulli beam is required to expand as the WKB series. The integral equation method has been formulated to give some approximate expressions for the fundamental frequency for Euler–Bernoulli beams as well as Rayleigh beams [11,24]. Although some methods are available for research on flapwise bending vibration of rotating tapered cantilevers, only numerical results have been given, in particular adopting the Euler–Bernoulli beam theory. So far there have not been any results reported on the use of the Rayleigh beam theory along with consideration of a distributed centrifugal shear force. Xi et al. [25] gave an analysis of free vibration of standing and hanging gravity-loaded Rayleigh cantilevers.

In this study, the integral equation method is further developed to analyze flapwise bending vibration of a rotating tapered Rayleigh beam where rotary inertia is taken into account. The problem is reduced to solving an integral equation, and the determination of natural frequencies is converted to an eigenvalue problem of a set of algebraic equations. Numerical results are confirmed and the dependence of the natural frequencies on the hub radius, rotational speed, taper ratio, and rotary inertia is elucidated. Obtained results are presented in tables and in graphs. In particular, the contribution of the natural frequencies resulting from a centrifugal shear force, $\rho I\Omega^2\partial w/\partial x$, is highlighted, which was often neglected.

2. Statement of the problem

Flapwise free vibration of a rotating blade is showed in Fig. 1, where the blade is modeled by a Rayleigh cantilever with variable cross-sections. Rotary inertia is considered. One end of the beam is fixed to a rigid hub with radius R, and the other end is free. The cantilever to be considered is assumed to rotate in the counter-clockwise direction at a constant angular velocity, Ω.

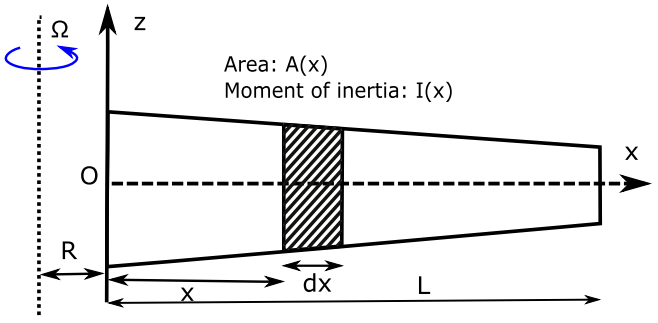

Fig. 1. Configuration of a rotating tapered cantilever beam.

For such a rotating Rayleigh beam that undergoes flapwise bending vibration, equation of motion can be obtained by using Hamilton's variational principle. To this end, the expression for the strain energy of a non-uniform beam due to flapwise bending is given by

$$W_1 = \frac{1}{2}\int_0^L EI(x)\left(\frac{\partial^2 w}{\partial x^2}\right)^2 dx, \tag{1}$$

where L is the length of the rotating beam in question, E is the modulus of elasticity, $I(x)$ is second moment of the cross-sectional area, and $w(x, t)$ is the flapwise bending displacement. The expression for the potential energy of a non-uniform beam due to rotation is given by

$$W_2 = \frac{1}{2}\int_0^L T(x)\left(\frac{\partial w}{\partial x}\right)^2 dx, \tag{2}$$

with

$$T(x) = \rho\Omega^2\int_x^L A(x)(R+x)dx, \tag{3}$$

where $T(x)$ is the centrifugal tension force at a distance x from the center of rotation, ρ is the mass density of the beam, $A(x)$ is variable cross-sectional area, and $\rho A(x)$ is variable mass per unit length of the beam. The expression for the kinetic energy of a non-uniform beam due to flapwise bending is given by

$$K_1 = \frac{1}{2}\int_0^L \rho A(x)\left(\frac{\partial w}{\partial t}\right)^2 dx. \tag{4}$$

Additionally, the kinetic energy of a non-uniform Rayleigh beam due to the rotary inertia is given by

$$K_2 = \frac{1}{2}\int_0^L \left[\rho I(x)\left(\frac{\partial^2 w}{\partial x\partial t}\right)^2 + \rho I(x)\Omega^2\left(\frac{\partial w}{\partial x}\right)^2\right] dx. \tag{5}$$

It is noted that the second term in the above integral arises from a result of the flapwise bending deformation since the positions at the cross-sections have different radii which make the particles at these positions experience different centrifugal force values although the net centrifugal force is independent of the cross-sectional rotation.

Thus, the Lagrangian function is given by

$$\begin{aligned} L &= K_1 + K_2 - W_1 - W_2 \\ &= \frac{1}{2}\int_0^L \left[\rho A(x)\left(\frac{\partial w}{\partial t}\right)^2 + \rho I(x)\left(\frac{\partial^2 w}{\partial x\partial t}\right)^2 + \rho I(x)\Omega^2\left(\frac{\partial w}{\partial x}\right)^2 - EI(x)\left(\frac{\partial^2 w}{\partial x^2}\right)^2 - T(x)\left(\frac{\partial w}{\partial x}\right)^2\right] dx. \end{aligned} \tag{6}$$

The equation of motion and associated boundary conditions are obtainable by applying Hamilton's principle that is expressed through the following variation

$$\delta\int_{t_1}^{t_2} L dt = 0, \tag{7}$$

where t_1 and t_2 stand for time. Performing variation manipulation, one finally obtains a governing equation for a rotating Rayleigh beam as follows

$$\frac{\partial^2}{\partial x^2}\left(EI\frac{\partial^2 w}{\partial x^2}\right) + \rho A(x)\frac{\partial^2 w}{\partial t^2} - \frac{\partial}{\partial x}\left(\rho I\frac{\partial^3 w}{\partial x\partial t^2}\right) - \frac{\partial}{\partial x}\left(T\frac{\partial w}{\partial x}\right) + \Omega^2\frac{\partial}{\partial x}\left(\rho I\frac{\partial w}{\partial x}\right) = 0, \tag{8}$$

and boundary conditions below

$$\frac{\partial^2 w}{\partial x^2}\delta\left(\frac{\partial w}{\partial x}\right)\Big|_0^L = 0, \qquad \left[\frac{\partial}{\partial x}\left(EI\frac{\partial^2 w}{\partial x^2}\right) - \rho I\frac{\partial^3 w}{\partial x \partial t^2} - T\frac{\partial w}{\partial x} + \rho I\Omega^2\frac{\partial w}{\partial x}\right]\delta w\Big|_0^L = 0. \tag{9}$$

Note that in rotating Euler–Bernoulli beams, rotary inertia is neglected, which is equivalent to setting $\rho I = 0$ in Eq. (8) along with Eq. (9) [2,3,11]. In addition, the last term in Eq. (8), $\Omega^2\frac{\partial}{\partial x}\left(\rho I\frac{\partial w}{\partial x}\right)$, describes a centrifugal shear force per unit length of the beam. It was not taken into account by some researchers such as [26] and [27]. As pointed out in [20], it is important, in particular for high rotational speeds [23]. Kaya [28] has studied the effect of this term.

As for the boundary conditions of a rotating cantilever, from Eq. (9) one easily gives

$$w = 0, \frac{\partial w}{\partial x} = 0, \qquad x = 0, \tag{10}$$

$$\frac{\partial^2 w}{\partial x^2} = 0, \frac{\partial}{\partial x}\left(EI\frac{\partial^2 w}{\partial x^2}\right) - \rho I\frac{\partial^3 w}{\partial x \partial t^2} + \rho I\Omega^2\frac{\partial w}{\partial x} = 0, \qquad x = L. \tag{11}$$

For uniform rotating Rayleigh beams, the above-derived governing equation reduces to

$$EI\frac{\partial^4 w}{\partial x^4} + \rho A\frac{\partial^2 w}{\partial t^2} - \rho I\frac{\partial^4 w}{\partial x^2 \partial t^2} - \frac{\partial}{\partial x}\left(T\frac{\partial w}{\partial x}\right) + \rho I\Omega^2\frac{\partial^2 w}{\partial x^2} = 0. \tag{12}$$

As a check, if letting rotational speed $\Omega = 0$, meaning the last two terms in (12) to disappear, from the above the well-known governing equation for Rayleigh beams is recovered.

3. Solution procedure

In this section, we present an integral equation method for solving the problem under consideration. For this purpose, we consider a general case of varying cross-section. That is, the cross-sectional area and its moment are assumed to respectively take the following expressions

$$A(x) = A_0\left(1 - c\frac{x}{L}\right)^n, \tag{13}$$

$$I(x) = I_0\left(1 - c\frac{x}{L}\right)^{n+m}, \tag{14}$$

where A_0, I_0 are the cross-sectional area and its moment of inertia at the hub, c is the taper ratio which satisfies $0 \le c < 1$, n and m are two constants reflecting the profile of various cross-sections. When taking different combined values of n and m, we get various shapes of the cross-section. For example, a cross-section with $n = 1$, $m = 0$ corresponds to a cantilever with constant depth and linearly varying width, and that with $n = 1$, $m = 2$ corresponds to a cantilever with constant width and linearly varying depth. The case of $n = m = 2$ represents a solid cone or pyramid-shaped cantilever, and so on. Clearly, the case of uniform beams can be recovered from $n = m = 0$. For most regular situations for non-uniform beams in practice, we often choose non-negative integers such as $n = 1$ or 2, $m = 0$, 1 or 2. In the following analysis, we restrict our attention to this case and denote $k = n + m$.

Substituting expressions Eqs. (13) and (14) into Eq. (8), the governing equation becomes

$$\begin{aligned} &EI_0\left(1-c\tfrac{x}{L}\right)^k\frac{\partial^4 w}{\partial x^4} - 2EI_0 k\frac{c}{L}\left(1-c\tfrac{x}{L}\right)^{k-1}\frac{\partial^3 w}{\partial x^3} \\ &+\Big[-\rho A_0\Omega^2\int_x^L\left(1-c\tfrac{x}{L}\right)^n(R+x)dx + \rho I_0\Omega^2\left(1-c\tfrac{x}{L}\right)^k \\ &+EI_0 k(k-1)\left(\tfrac{c}{L}\right)^2\left(1-c\tfrac{x}{L}\right)^{k-2}\Big]\frac{\partial^2 w}{\partial x^2} \\ &+\left[\rho A_0\Omega^2(R+x)\left(1-c\tfrac{x}{L}\right)^n - \rho I_0 k\Omega^2\frac{c}{L}\left(1-c\tfrac{x}{L}\right)^{k-1}\right]\frac{\partial w}{\partial x} - \rho I_0\left(1-c\tfrac{x}{L}\right)^k\frac{\partial^4 w}{\partial x^2\partial t^2} \\ &+\rho I_0 k\frac{c}{L}\left(1-c\tfrac{x}{L}\right)^{k-1}\frac{\partial^3 w}{\partial x\partial t^2} + \rho A_0\left(1-c\tfrac{x}{L}\right)^n\frac{\partial^2 w}{\partial t^2} = 0. \end{aligned} \tag{15}$$

Since free vibration is considered, simple harmonic oscillation is of interest to us and then $w(x, t)$ can be assumed to take the form

$$w(x,t) = Y(x)e^{i\omega t}, \tag{16}$$

where $Y(x)$ is the amplitude of vibration, ω is the angular frequency. Substituting Eq. (16) into Eq. (15) yields an ordinary differential equation for Y

$$\begin{aligned} &EI_0\left(1-c\tfrac{x}{L}\right)^k\frac{d^4 Y}{dx^4} - 2EI_0\frac{c}{L}(n+2)\left(1-c\tfrac{x}{L}\right)^{k-1}\frac{d^3 Y}{dx^3} \\ &+\Big[-\rho A_0\Omega^2\int_x^L\left(1-c\tfrac{x}{L}\right)^n(R+x)dx + \rho I_0\left(\Omega^2+\omega^2\right)\left(1-c\tfrac{x}{L}\right)^k \\ &+EI_0\left(\tfrac{c}{L}\right)^2 k(k-1)\left(1-c\tfrac{x}{L}\right)^{k-2}\Big]\frac{d^2 Y}{dx^2} \\ &+\left[\rho A_0\Omega^2(R+x)\left(1-c\tfrac{x}{L}\right)^n - \rho I_0\left(\Omega^2+\omega^2\right)\frac{c}{L}k\left(1-c\tfrac{x}{L}\right)^{k-1}\right]\frac{dY}{dx} \\ &-\rho A_0\omega^2\left(1-c\tfrac{x}{L}\right)^n Y = 0. \end{aligned} \tag{17}$$

Accordingly substituting Eqs. (13), (14), and (16) into Eqs. (10) and (11) results in the cantilever boundary conditions

$$Y = 0, \frac{dY}{dx} = 0, \qquad x = 0, \tag{18}$$

$$\frac{d^2 Y}{dx^2} = 0, EI_0\frac{d^3 Y}{dx^3} + \rho I_0\Omega^2\left(\Omega^2+\omega^2\right)\frac{dY}{dx} = 0, \qquad x = L. \tag{19}$$

For convenience of analysis, we denote

$$\begin{aligned} &\xi = \frac{x}{L}, \qquad U(\xi) = \frac{Y(x)}{L}, \qquad r_0 = \frac{R}{L}, \\ &r^2 = \frac{I_0}{A_0 L^2}, \quad \eta^2 = \frac{\rho A_0}{EI_0}\Omega^2 L^4, \quad \lambda^2 = \frac{\rho A_0}{EI_0}\omega^2 L^4, \end{aligned} \tag{20}$$

where ξ, U and r_0 are the dimensionless parameters for the local location, the amplitude, and the hub radius, respectively, r, η and λ are the dimensionless parameters related to the inverse of slenderness ratio, the angular velocity and the angular frequency, respectively. After lengthy algebraic manipulation, with the help of expressions in Eq. (20), Eq. (17) can be rewritten as a fourth-order ordinary differential equation with variable coefficients

$$\begin{aligned} &(1-c\xi)^k\frac{d^4 U}{d\xi^4} - 2ck(1-c\xi)^{k-1}\frac{d^3 U}{d\xi^3} + \Big[c^2 k(k-1)(1-c\xi)^{k-2} \\ &-\eta^2\int_\xi^1(1-c\xi)^n(r_0+\xi)d\xi + r^2\left(\eta^2+\lambda^2\right)(1-c\xi)^k\Big]\frac{d^2 U}{d\xi^2} + [\eta^2(r_0+\xi)(1-c\xi)^n \\ &-cr^2\left(\eta^2+\lambda^2\right)k(1-c\xi)^{k-1}\Big]\frac{dU}{d\xi} - \lambda^2(1-c\xi)^n U = 0. \end{aligned} \tag{21}$$

In addition, the above equation is solved under appropriate boundary conditions. For the present study, the solution must satisfy Eqs. (18) and (19), which can be expressed in terms of the above-introduced dimensionless variables

$$U = 0, \frac{dU}{d\xi} = 0, \qquad \xi = 0, \tag{22}$$

Table 1
First four dimensionless natural frequencies for a non-rotating uniform beam with $r_0 = 0$, $\eta = 0$, $n = m = 0$.

No. of modes	Euler–Bernoulli beam ($r = 0$)		Rayleigh beam ($r = 1/20$)		Rayleigh beam ($r = 1/10$)	
	Present	[30]	Present	[29]	Present	[29]
First	3.51602	3.5160	3.49575	3.4957	3.43681	3.4363
Second	22.03449	22.0345	21.19069	21.1907	19.13637	19.1364
Third	61.69721	61.6972	56.48626	56.4863	46.49355	46.49355
Fourth	120.90206	120.902	103.82380	103.8238	78.21309	78.2131

$$\frac{d^2U}{d\xi^2} = 0, \frac{d^3U}{d\xi^3} + r^2\left(\eta^2 + \lambda^2\right)\frac{dU}{d\xi} = 0, \qquad \xi = 1. \tag{23}$$

In order to reduce the order of the differential Eq. (21), we introduce a function $V(\xi)$ such that

$$V(\xi) = \frac{d^2U}{d\xi^2}. \tag{24}$$

Clearly, the amplitude U can be determined from the following integrals

$$\frac{dU}{d\xi} = \int_0^\xi V(s)ds, \tag{25}$$

$$U = \int_0^\xi (\xi - s)V(s)ds. \tag{26}$$

Thus the remaining two boundary conditions in Eq. (23) become

$$V(1) = 0, \tag{27}$$

$$\left.\frac{dV}{d\xi}\right|_{\xi=1} = -r^2\left(\eta^2 + \lambda^2\right)\int_0^1 V(s)ds. \tag{28}$$

Next, inserting Eqs. (24), (25), and (26) into Eq. (21) leads to

$$(1-c\xi)^k\frac{d^2V}{d\xi^2} - 2ck(1-c\xi)^{k-1}\frac{dV}{d\xi} + \left[c^2k(k-1)(1-c\xi)^{k-2} - \eta^2\int_\xi^1 (1-c\xi)^n(r_0+\xi)d\xi + r^2\left(\eta^2+\lambda^2\right)(1-c\xi)^k\right]V + \int_0^\xi H(\xi,s)V(s)ds = 0, \tag{29}$$

where

$$H(\xi,s) = \eta^2(r_0+\xi)(1-c\xi)^n - cr^2\left(\eta^2+\lambda^2\right)k(1-c\xi)^{k-1} - \lambda^2(1-c\xi)^n(\xi-s). \tag{30}$$

To further simplify our solution procedure, we introduce $K_a^b(\xi)$, $J_c^d(\xi)$ and $M_{a,b}^{c,d}(\xi)$ to respectively express

$$K_a^b(\xi) = \xi^a(1-c\xi)^b, \tag{31}$$

$$J_a^b(\xi) = \int_0^\xi s^a(1-cs)^b V(s)ds, \tag{32}$$

$$M_{a,b}^{c,d}(\xi) = K_a^b(\xi)J_c^d(\xi) - J_{a+c}^{b+d}(\xi), \tag{33}$$

$$P_{a,b}^{c,d}(\xi) = M_{a,b}^{c,d}(\xi) - M_{a,b}^{c,d}(1). \tag{34}$$

Integrating both sides of Eq. (29) twice with respect to ξ results in

$$\begin{aligned} &c^2(n+1)(n+2)(1-c\xi)^{k-1}\left[(1-c\xi)\frac{dV}{d\xi} - ckV\right] \\ &+\lambda^2\left\{(n+2)\left(M_{0,n+1}^{0,0} - cM_{0,n+1}^{1,0}\right) - (n+1)M_{0,n+2}^{0,0}\right\} \\ &+c^2r^2(n+1)(n+2)\left(\eta^2+\lambda^2\right)K_0^kJ_0^0 + \eta^2(n+1)K_0^{n+2}J_0^0 \\ &-\eta^2(n+2)(cr_0+1)K_0^{n+1}J_0^0 + \eta^2(1-c)^{n+1}[(n+2)cr_0 + (n+1)c + 1]J_0^0 = C_1, \end{aligned} \tag{35}$$

and

$$\begin{aligned} &c^2(n+1)(n+2)(1-c\xi)^kV - \lambda^2\left[(n+2)\left(M_{1,0}^{0,n+1} - cM_{1,0}^{1,n+1}\right) - (n+1)M_{1,0}^{0,n+2}\right] \\ &+\frac{(cr_0+1)\eta^2-\lambda^2}{c}M_{0,n+2}^{0,0} + \eta^2(1-c)^{n+1}[(n+2)cr_0 + (n+1)c + 1]M_{1,0}^{0,0} + \lambda^2M_{0,n+2}^{1,0} \\ &-\frac{cr^2(n+1)(n+2)\left(\eta^2+\lambda^2\right)}{k+1}M_{0,k+1}^{0,0} - \frac{(n+1)\left(\eta^2-\lambda^2\right)}{(n+3)c}M_{0,n+3}^{0,0} = C_1\xi + C_2, \end{aligned} \tag{36}$$

where C_1 and C_2 are two integration constants, which can be determined via appropriate boundary conditions. In what follows we apply the boundary conditions in Eqs. (27) and (28) to Eq. (35), yielding

$$C_1 = \lambda^2\left\{(n+2)\left[M_{0,n+1}^{0,0}(1) - cM_{0,n+1}^{1,0}(1)\right] - (n+1)M_{0,n+2}^{0,0}(1)\right\}. \tag{37}$$

Furthermore, substituting $V(1) = 0$ and Eq. (37) into Eq. (36) yields

$$\begin{aligned} C_2 = {} &\eta^2(1-c)^{n+1}[(n+2)cr_0 + (n+1)c + 1]M_{1,0}^{0,0}(1) - \frac{cr^2(n+1)(n+2)\left(\eta^2+\lambda^2\right)}{k+1}M_{0,k+1}^{0,0}(1) \\ &+\lambda^2(n+2)\left\{c\left[M_{1,0}^{1,n+1}(1) + M_{0,n+1}^{1,0}(1)\right] - \left[M_{1,0}^{0,n+1}(1) + M_{0,n+1}^{0,0}(1)\right]\right\} + \lambda^2(n+1)M_{1,0}^{0,n+2}(1) \\ &-\frac{(n+1)\left(\eta^2-\lambda^2\right)}{(n+3)c}M_{0,n+3}^{0,0}(1) + \frac{(cr_0+1)\eta^2 - \lambda^2(1-c-nc)}{c}M_{0,n+2}^{0,0}(1). \end{aligned} \tag{38}$$

Table 2
First three dimensionless natural frequencies of a rotating tapered beam with $n = 1$, $m = 2$, $c = 0.5$, $r = 0$ (Euler–Bernoulli theory), 1/30 (Rayleigh theory).

	$\eta = 1$			$\eta = 2$			$\eta = 3$			$\eta = 4$		
	EB	EB [3]	Rayleigh	EB	EB [3]	Rayleigh	EB	EB [3]	Rayleigh	EB	EB [3]	Rayleigh
$r_0 = 0$												
λ_1	3.98662	3.98662	3.98024	4.43680	4.43680	4.42885	5.09267	5.09268	5.08260	5.87876	5.87796	5.86636
λ_2	18.47401	18.47400	18.32386	18.93663	18.93660	18.78129	19.68390	19.68390	19.52026	20.68516	20.68500	20.51055
λ_3	47.41728	47.41700	46.47541	47.87162	47.87160	46.91902	48.61901	48.61890	47.64878	49.64564	49.64560	48.65120
$r_0 = 2$												
λ_1	4.38668	4.38668	4.37977	5.74259	5.74260	5.73313	7.45274	7.45275	7.44031	9.31032	9.31032	9.29482
λ_2	18.87955	18.87950	18.72593	20.47302	20.47300	20.30461	22.87948	22.87400	22.68885	25.86626	25.86624	25.64817
λ_3	47.83075	47.83080	46.88033	49.48668	49.48660	48.50065	52.12055	52.12050	51.07763	55.58170	55.58160	54.46344

Table 3
First three dimensionless natural frequencies of a rotating tapered beam with $n = 1$, $m = 2$, $r_0 = 0$.

		λ_1							λ_2							λ_3						
		$c = 0$	$c = 0.25$		$c = 0.5$		$c = 0.75$		$c = 0$	$c = 0.25$		$c = 0.5$		$c = 0.75$		$c = 0$	$c = 0.25$		$c = 0.5$		$c = 0.75$	
η	$1/r$	Present	Present	[22]	Present	[22]	Present	[22]	Present	Present	[22]	Present	[22]	Present	[22]	Present	Present	[22]	Present	[22]	Present	[22]
0	10	3.4368	3.5722	3.5722	3.7727	3.7727	4.1348	4.1348	19.1364	18.2726	18.273	17.0975	17.097	15.5439	15.544	46.4936	43.9430	43.943	40.4125	40.412	35.2608	35.261
	30	3.5070	3.6290	3.6290	3.8180	3.8180	4.1719	4.1719	21.6477	20.0022	20.002	18.1689	18.169	16.1092	16.109	59.2073	53.1494	53.149	46.3266	46.327	38.3323	38.332
	50	3.5128	3.6336	3.6336	3.8217	3.8217	4.1749	4.1749	21.8929	20.1622	20.162	18.2634	18.263	16.1571	16.157	60.7649	54.1687	54.169	46.9205	46.921	38.6138	38.614
	100	3.5152	3.6356	3.6356	3.8233	3.8233	4.1762	4.1762	21.9989	20.2309	20.231	18.3038	18.304	16.1775	16.177	61.4601	54.6166	54.617	47.1780	47.178	38.7344	38.735
	EB	3.5160	3.6362	3.6362	3.8238	3.8238	4.1766	4.1766	22.0345	20.2539	20.254	18.3173	18.317	16.1843	16.184	61.6972	54.7684	54.768	47.2648	47.265	38.7749	38.775
5	10	6.2318	6.3958	6.3958	6.6118	6.6118	6.9577	6.9577	21.8856	21.2756	21.276	20.3563	20.356	19.0586	19.059	48.9470	46.6548	46.654	43.4436	43.444	38.6896	38.690
	30	6.4251	6.5469	6.5469	6.7286	6.7286	7.0506	7.0506	24.9737	23.4339	23.434	21.7176	21.718	19.7978	19.798	62.5392	56.5937	56.594	49.9090	49.909	42.1175	42.118
	50	6.4407	6.5591	6.5591	6.7381	6.7381	7.0581	7.0581	25.2734	23.6325	23.632	21.8372	21.837	19.8603	19.860	64.2069	57.6940	57.694	50.5578	50.558	42.4314	42.432
	100	6.4473	6.5643	6.5643	6.7421	6.7421	7.0613	7.0613	25.4026	23.7176	23.718	21.8882	21.888	19.8869	19.887	64.9512	58.1776	58.178	50.8390	50.839	42.5658	42.566
	EB	6.4495	6.5660	6.5660	6.7434	6.7434	7.0623	7.0623	25.4461	23.7462	23.746	21.9053	21.905	19.8958	19.896	65.2050	58.3414	58.341	50.9338	50.934	42.6109	42.611
10	10	10.8187	11.0217	11.022	11.2631	11.263	11.6095	11.610	28.4787	28.3901	28.390	27.9160	27.916	26.9155	26.915	55.4945	53.8431	53.843	51.3960	51.396	47.4782	47.478
	30	11.1598	11.2889	11.289	11.4748	11.475	11.7887	11.789	32.9654	31.5417	31.542	29.9097	29.910	28.0186	28.019	71.4977	65.7662	65.766	59.3123	59.312	51.8008	51.801
	50	11.1870	11.3104	11.310	11.4919	11.492	11.8032	11.803	33.3940	31.8280	31.828	30.0838	30.084	28.1118	28.112	73.4696	67.0859	67.086	60.1048	60.105	52.1958	52.196
	100	11.1985	11.3195	11.320	11.4991	11.499	11.8093	11.809	33.5784	31.9506	31.951	30.1579	30.158	28.1514	28.151	74.3493	67.6656	67.666	60.4482	60.448	52.3651	52.365
	EB	11.2023	11.3225	11.323	11.5015	11.502	11.8113	11.811	33.6404	31.9917	31.992	30.1827	30.183	28.1646	28.164	74.6493	67.8620	67.862	60.5639	60.564	52.4218	52.422

Table 4
First three dimensionless natural frequencies of a rotating tapered beam with $n = m = 2$, $r_0 = 0$.

		λ_1							λ_2							λ_3						
		$c = 0$	$c = 0.25$		$c = 0.5$		$c = 0.75$		$c = 0$	$c = 0.25$		$c = 0.5$		$c = 0.75$		$c = 0$	$c = 0.25$		$c = 0.5$		$c = 0.75$	
η	$1/r$	Present	Present	[22]	Present	[22]	Present	[22]	Present	Present	[22]	Present	[22]	Present	[22]	Present	Present	[22]	Present	[22]	Present	[22]
0	10	3.4368	3.8824	3.8824	4.5517	4.5517	5.7394	5.7394	19.1364	18.7656	18.766	18.2107	18.211	17.6638	17.664	46.4936	44.3682	44.368	41.4572	41.457	37.4027	37.403
	30	3.5070	3.9483	3.9483	4.6168	4.6168	5.8136	5.8136	21.6477	20.5475	20.548	19.3846	19.385	18.3834	18.384	59.2073	53.6911	53.691	47.6021	47.602	40.8245	40.825
	50	3.5128	3.9537	3.9537	4.6221	4.6221	5.8196	5.8196	21.8929	20.7125	20.713	19.4885	19.489	18.4449	18.445	60.7649	54.7231	54.723	48.2204	48.220	41.1401	41.141
	100	3.5152	3.9559	3.9559	4.6244	4.6244	5.8222	5.8222	21.9989	20.7832	20.783	19.5328	19.533	18.4710	18.471	61.4601	55.1767	55.177	48.4885	48.489	41.2755	41.276
	EB	3.5160	3.9567	3.9567	4.6252	4.6252	5.8231	5.8231	22.0345	20.8069	20.807	19.5476	19.548	18.4797	18.480	61.6972	55.3304	55.330	48.5789	48.579	41.3209	41.321
5	10	6.2318	6.5881	6.5881	7.1268	7.1268	8.0992	8.0992	21.8856	21.5647	21.565	21.0033	21.003	20.3879	20.388	48.9470	46.8699	46.870	44.0143	44.014	40.0105	40.011
	30	6.4251	6.7521	6.7521	7.2717	7.2717	8.2436	8.2436	24.9737	23.7497	23.750	22.4375	22.438	21.2663	21.266	62.5392	56.8774	56.877	50.6397	50.640	43.7292	43.730
	50	6.4407	6.7654	6.7654	7.2835	7.2835	8.2554	8.2554	25.2734	23.9509	23.951	22.5640	22.564	21.3411	21.341	64.2069	57.9848	57.985	51.3057	51.306	44.0719	44.072
	100	6.4473	6.7711	6.7711	7.2885	7.2885	8.2604	8.2604	25.4026	24.0371	24.037	22.6179	22.618	21.3729	21.373	64.9512	58.4715	58.472	51.5945	51.595	44.2188	44.219
	EB	6.4495	6.7729	6.7729	7.2901	7.2901	8.2620	8.2620	25.4461	24.0660	24.066	22.6360	22.636	21.3836	21.384	65.2050	58.6364	58.636	51.6918	51.692	44.2681	44.269
10	10	10.8187	11.1593	11.159	11.6467	11.647	12.4866	12.487	28.4787	28.3154	28.315	27.7327	27.733	26.8986	26.899	55.4945	53.5748	53.575	50.8800	50.880	46.9565	46.957
	30	11.1598	11.4490	11.449	11.9083	11.908	12.7568	12.767	32.9654	31.4425	31.443	29.7521	29.752	28.1364	28.136	71.4977	65.4472	65.447	58.7878	58.788	51.4492	51.450
	50	11.1870	11.4724	11.472	11.9295	11.930	12.7788	12.779	33.3940	31.7269	31.727	29.9292	29.929	28.2417	28.242	73.4696	66.7598	66.760	59.5805	59.581	51.8625	51.863
	100	11.1985	11.4823	11.482	11.9385	11.939	12.7881	12.788	33.5784	31.8487	31.849	30.0046	30.005	28.2864	28.287	74.3493	67.3363	67.336	59.9241	59.924	52.0397	52.040
	EB	11.2023	11.4856	11.486	11.9415	11.942	12.7912	12.791	33.6404	31.8895	31.890	30.0299	30.030	28.3014	28.301	74.6493	67.5316	67.532	60.0399	60.040	52.0992	52.100

Inserting the expressions (37) and (38) into Eq. (36) leads to

$$\begin{aligned}
&c^2(n+1)(n+2)(1-c\xi)^k V-\lambda^2(n+2)\left\{P_{1,0}^{0,n+1}-cP_{1,0}^{1,n+1}+(\xi-1)\left[M_{0,n+1}^{0,0}(1)-cM_{0,n+1}^{1,0}(1)\right]\right\}\\
&+\lambda^2 M_{0,n+2}^{1,0}+\lambda^2(n+1)\left[P_{1,0}^{0,n+2}+(\xi-1)M_{0,n+2}^{0,0}(1)\right]\\
&+\frac{(cr_0+1)\eta^2-\lambda^2}{c}P_{0,n+2}^{0,0}-\frac{(n+1)\left(\eta^2-\lambda^2\right)}{(n+3)c}P_{0,n+3}^{0,0}\\
&+\eta^2(1-c)^{n+1}[(n+2)cr_0+(n+1)c+1]P_{1,0}^{0,0}\\
&-\frac{cr^2(n+1)(n+2)\left(\eta^2+\lambda^2\right)}{k+1}P_{0,k+1}^{0,0}=0.
\end{aligned}\tag{39}$$

Thus we have derived an integral Eq. (39). To obtain a nontrivial solution of the above integral equation, considering $V(1)=0$, we assume $V(\xi)$ as a power series in ξ, which is written as an alternative form

$$V(\xi)=\sum_{i=1}^{N}A_i\left(1-\xi^i\right),\qquad 0\le\xi\le1,\tag{40}$$

where A_i's are unknown coefficients, and N is a positive integer. Substituting the expression Eq. (40) into Eq. (39) yields

$$\sum_{i=1}^{N}D_i(\xi)A_i=0,\tag{41}$$

where

$$\begin{aligned}
D_i(\xi)=&\left\{\lambda^2(n+1)\left[P_{1,0}^{0,n+2}+(\xi-1)M_{0,n+2}^{0,0}(1)\right]+\frac{(cr_0+1)\eta^2-\lambda^2}{c}P_{0,n+2}^{0,0}\right.\\
&-\frac{(n+1)\left(\eta^2-\lambda^2\right)}{(n+3)c}P_{0,n+3}^{0,0}+c^2(n+1)(n+2)(1-c\xi)^kV\\
&-\lambda^2(n+2)(\xi-1)\left[M_{0,n+1}^{0,0}(1)-cM_{0,n+1}^{1,0}(1)\right]-\lambda^2(n+2)\left(P_{1,0}^{0,n+1}-cP_{1,0}^{1,n+1}\right)\\
&+\eta^2(1-c)^{n+1}[(n+2)cr_0+(n+1)c+1]P_{1,0}^{0,0}\\
&\left.-\frac{cr^2(n+1)(n+2)\left(\eta^2+\lambda^2\right)}{k+1}P_{0,k+1}^{0,0}+\lambda^2M_{0,n+2}^{1,0}\right\}_{V=1-\xi^i}.
\end{aligned}\tag{42}$$

Eq. (41) may be understood as a system of algebraic equation with N unknowns. Since the coefficients are functions depending on ξ, the solution can be approximately determined by multiplying both sides of Eq. (41) by ξ^{j-1} ($j=1, 2 \ldots N$) and then integrating each equation with respect to ξ from 0 to 1. After some algebraic calculation, one finally gets

$$\sum_{i=1}^{N}K_{ji}A_i=0,\qquad j=1,2,3\ldots N,\tag{43}$$

Table 6
Effect of the $\rho I\Omega^2\partial w/\partial x$ term on the natural frequencies with $c=0.5$, $n=1$, $m=2$, $r_0=0$, $r=1/30$.

η		With the term	[22]	Without the term	Error (%)
0	λ_1	3.81801	3.8180	3.81801	0
	λ_2	18.16889	18.169	18.16889	0
	λ_3	46.32655	46.327	46.32655	0
	λ_4	87.13706		87.13706	0
	λ_5	139.47775		139.47775	0
5	λ_1	6.72860	6.7286	6.73386	0.07808
	λ_2	21.71756	21.718	21.72690	0.04301
	λ_3	49.90902	49.909	49.91891	0.01980
	λ_4	90.74262		90.75254	0.01093
	λ_5	143.05892		143.06869	0.00683
10	λ_1	11.47479	11.475	11.48632	0.10047
	λ_2	29.90969	29.910	29.93684	0.09076
	λ_3	59.31229	59.312	59.34587	0.05662
	λ_4	100.73094		100.76676	0.03557
	λ_5	153.26577		153.30225	0.02380

where

$$K_{ji}=\int_0^1\xi^{j-1}D_i(\xi)d\xi.\tag{44}$$

Hence, it is a system of linear algebraic equations in A_i ($i=1, 2 \ldots N$) with constant coefficients. To ensure the existence of a nontrivial solution of the system Eq. (43), the determinant of the coefficient matrix must be zero. Consequently, one obtains the frequency equation in λ^2 expressed as

$$\det\left[K_{ji}\right]=0.\tag{45}$$

As a result, the natural frequencies of a rotating Rayleigh cantilever can be calculated by solving the frequency Eq. (45).

4. Results and discussion

In this section, illustrative examples are given to show the influence of the geometry parameters and rotational speed on the natural frequencies. Prior to the presentation of our numerical results, let us first consider a simple uniform non-rotating beam to confirm the effectiveness of the present approach. We set $n=m=0$, $\eta=0$, $r_0=0$. The taper ratio c may be chosen as an arbitrary constant, $c=0.5$, say. Taking $r=0$ for an Euler–Bernoulli beam and $r=1/20$ or $1/10$ for a Rayleigh beam, respectively, we calculate the first four dimensionless frequencies by selecting $N=10$ and obtained numerical results are tabulated in Table 1. From Table 1, we can see that the numerical results coincide well with the known ones [29,30]. This indicates that the method

Table 5
First five dimensionless natural frequencies of a rotating tapered beam with $n=3$, $m=2$, $c=0.5$, $r=0$ (Euler–Bernoulli theory), 1/30 (Rayleigh theory).

	$\eta=0$		$\eta=2$		$\eta=4$		$\eta=6$		$\eta=8$		$\eta=10$	
	EB	Rayleigh	EB	Rayleigh	EB	Rayleigh	EB	Rayleigh	EB	Rayleigh	EB	Rayleigh
$r_0=0$												
λ_1	5.545852	5.218713	6.007995	5.615210	7.201421	6.651426	8.801007	8.058103	10.595828	9.649077	12.483648	11.328488
λ_2	20.870368	16.883459	21.322579	17.205989	22.625718	18.140622	24.644740	19.602129	27.216341	21.482831	30.191682	23.679008
λ_3	50.015803	33.258560	50.454246	33.510842	51.746932	34.255752	53.831132	35.459827	56.617105	37.074104	60.003519	39.041570
λ_4	93.312501	50.969097	93.747888	51.176391	95.041611	51.793007	97.157963	52.803704	100.042374	54.184809	103.627427	55.906399
λ_5	150.914254	69.034150	151.349241	69.209018	152.646409	69.731011	154.783020	70.592472	157.723175	71.781188	161.420468	73.281135
$r_0=2$												
λ_1	5.545852	5.218713	7.127170	6.677619	10.481072	9.792374	14.361705	13.409967	18.413808	17.191927	22.536234	21.040568
λ_2	20.870368	16.883459	22.509423	18.159363	26.825723	21.528694	32.754356	26.165094	39.547933	31.471977	46.809864	37.123502
λ_3	50.015803	33.258560	51.668862	34.310235	56.325066	37.270127	63.293865	41.686285	71.867807	47.082324	81.508061	53.082575
λ_4	93.312501	50.969097	94.991336	51.859198	99.847936	54.438104	107.423320	58.469396	117.150978	63.653741	128.499736	69.701163
λ_5	150.914254	69.034150	152.614269	69.794855	157.597079	72.030179	165.545561	75.612491	176.025698	80.364084	188.575284	86.090602

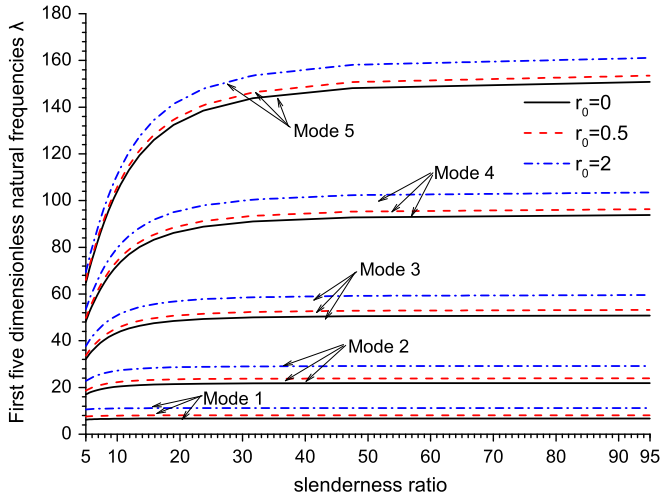

Fig. 2. First five dimensionless natural frequencies as a function of slenderness ratio with $c = 0.5, \eta = 5$ and three different hub radii $r_0 = 0, 0.5, 2$.

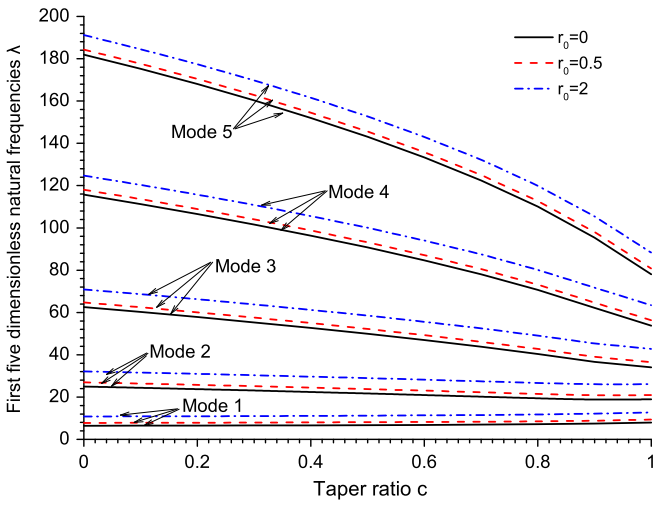

Fig. 4. First five dimensionless natural frequencies as a function of the taper ratio c with various hub radii.

described in this paper is efficient. In the following, we also select $N = 10$ unless otherwise stated.

4.1. Example 1. Beams with linearly varying depth and constant width

Example 1 is devoted to a Rayleigh beam with linearly varying depth and constant width, corresponding to $n = 1$, $m = 2$. In this case, the cross-sectional area and its moment have the following expressions

$$A(\xi) = A_0(1-c\xi), \tag{46}$$

$$I(\xi) = I_0(1-c\xi)^3. \tag{47}$$

For four different rotational speeds, $\eta = 1, 2, 3, 4$, we calculate the first three dimensionless natural frequencies for a rotating Euler–Bernoulli beam when choosing $c = 0.5$, $r = 0$, $r_0 = 0, 2$, and obtained results are presented in Table 2. Also we list the previous results [3] in Table 2 and find that our numerical results agree with those in [3]. When taking rotary inertia into account, the corresponding frequencies according to the Rayleigh beam theory are determined when taking $r = 1/30$ instead of $r = 0$. From Table 2, it is viewed that consideration of rotary inertia gives rise to a reduction of the natural frequencies. This agrees with what we expect. Moreover, we can see that the rotational speed and hub radius have great effects on the natural frequencies, and it indicates that for $\eta \neq 0$, the natural frequencies increase as the hub radius and rotating velocity increase. This is due to the increasing of centrifugal force as the rotational speed and hub radius increase, coinciding with that in [15]. The increasing of centrifugal force gives rise to the increase of natural frequencies due to the stiffening effect of rotation.

For three different rotational speeds, $\eta = 0, 5, 10$, and three different taper ratios, $c = 0.25, 0.5, 0.75$, the first three dimensionless natural frequencies are calculated for rotating Rayleigh and Euler–Bernoulli beams where the hub radius was set to zero, and obtained results are tabulated in Table 3. Note that the results for Euler–Bernoulli beams ($r = 0$) are shown in the rows marked with EB. The difference between the results of Rayleigh beams and Euler–Bernoulli beams is gradually apparent for short beams ($1/r$ is small enough). The effect of rotary inertia on the natural frequencies has the same trend as said before. By comparing with the previous results [22], we find that the present results have a good agreement with those in [22].

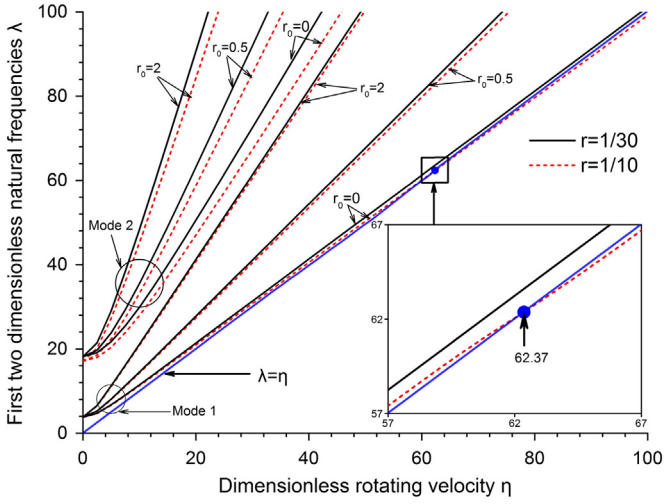

Fig. 3. First two dimensionless natural frequencies as a function of the rotating velocity η with different values of r_0 and r.

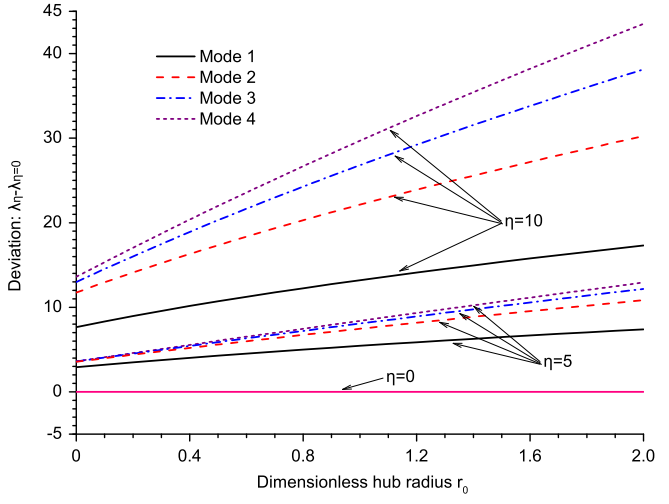

Fig. 5. Increment of first four dimensionless natural frequencies as a function of the hub radius r_0 with various rotating velocities.

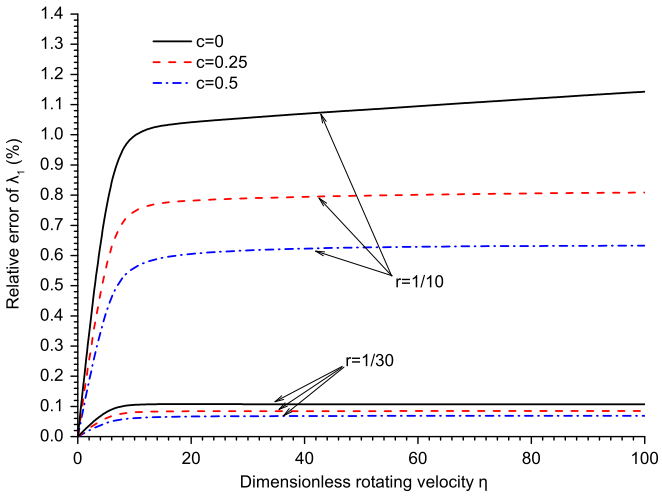

Fig. 6. Relative error of the first dimensionless natural frequencies as a function of the rotating velocity η with various values of r and c.

4.2. Example 2. Beams with linearly varying depth and width

In this example, we consider a rotating beam with linearly varying depth and width, which corresponds to $n = 2$, $m = 2$. Accordingly, the cross-sectional area and its moment have the following expressions

$$A(\xi) = A_0(1-c\xi)^2, \tag{48}$$

$$I(\xi) = I_0(1-c\xi)^4. \tag{49}$$

For rotating Euler–Bernoulli and Rayleigh beams, we choose the same dimensionless parameters as those used in Table 3, and evaluate the first three dimensionless frequencies for various gyration radii. Obtained numerical results are shown in Table 4, and they coincide well with those in [22]. This confirms the accuracy of the integral equation method again. Consideration of rotary inertia gives rise to a reduction of the natural frequencies, while the increase of rotational speed leads to an increase of the natural frequencies. For Rayleigh and Euler–Bernoulli beams, comparing the results of Table 4 with Table 3, it can be found that the effect of rotary inertia on natural frequencies is slightly more significant for $n = 2$.

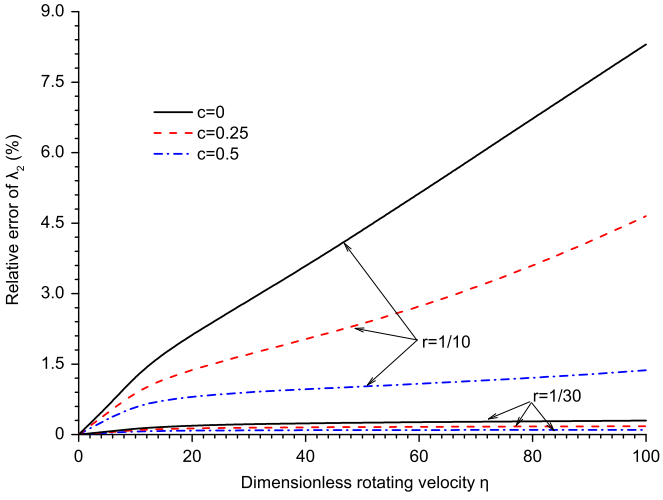

Fig. 7. Relative error of the second dimensionless natural frequencies as a function of the rotating velocity η with various values of r and c.

4.3. Example 3. Beams with linearly varying depth and parabolically varying width

A rotating beam with linearly varying depth and parabolically varying width corresponding to $n = 3$, $m = 2$ is considered in this example. The cross-sectional area and its moment have the following expressions:

$$A(\xi) = A_0(1-c\xi)^3, \tag{50}$$

$$I(\xi) = I_0(1-c\xi)^5, \tag{51}$$

For six different rotational speeds, $\eta = 0, 2, ..., 10$, the first five dimensionless natural frequencies for rotating Euler–Bernoulli and Rayleigh beams are tabulated in Table 5, where the dimensionless parameters are chosen as $c = 0.5$, $r = 0, 1/30$, $r_0 = 0, 2$. Here the results for $r = 0$ correspond to those for Euler–Bernoulli beams, whereas those for $r = 1/30$ correspond to those for Rayleigh beams. Similar to the trend observed before, from Table 5 consideration of rotary inertia gives rise to a reduction of the natural frequencies. The hub radius has no effect on the natural frequencies for a non-rotating beam ($\eta = 0$), which is what we expect.

Next, we turn our attention to the effect of $\rho I\Omega^2 \partial w/\partial x$ on the natural frequencies. For convenience, we still choose the following dimensionless parameters: $c = 0.5$, $n = 1$, $m = 2$, $r_0 = 0$, $r = 1/30$ and different rotational speeds. Calculated results including and excluding the effect of the term, $\rho I\Omega^2 \partial w/\partial x$, are listed in Table 6. From Table 6, we find that the present results including the effect of the $\rho I\Omega^2 \partial w/\partial x$ term are closer to the known results in [22]. Moreover, the natural frequencies are slightly lower than those when neglecting the contribution of the $\rho I\Omega^2 \partial w/\partial x$ term. This conclusion agrees with that in [20]. Obviously, with rotational speeds rising, the influence becomes larger, in particular for the fundamental frequencies. Therefore, for a cantilever beam rotating with high speed, it is necessary to take the $\rho I\Omega^2 \partial w/\partial x$ term into consideration in accurately calculating the natural frequencies.

The effects of different dimensionless parameters on the natural frequencies are examined in what follows. As a representative, we only present illustrative graphs for the case of $n = 1$, $m = 2$, i.e. a rotating beam with linearly varying depth and constant width.

Fig. 2 shows the first five dimensionless natural frequencies as a function of slenderness ratio with $c = 0.5$, $\eta = 5$, and three different hub radii $r_0 = 0$, 0.5 and 2. According to the definition of r in Eq. (20), r actually stands for the inverse of the slenderness ratio of a beam with uniform cross-section. From Fig. 2, it is found that the natural frequencies decrease with the increase of r, implying that consideration of rotary inertia causes the natural frequencies to drop. In other words, for short rotating beams, the natural frequencies are overestimated if neglecting rotary inertia. In contrast, for a rotating beam (i.e. $\eta \neq 0$), with the increase of hub radius, the natural frequencies become large. This is due to the cause of the increase of centrifugal force resulting from the increase of hub radius. In this case, the rotating beams seem to become stiffer.

Fig. 3 displays the first two dimensionless natural frequency curves against the dimensionless rotational speed η with a special taper ratio $c = 0.5$ and three different hub radii $r_0 = 0, 0.5, 2$. In calculating numerical results, two different values of r, $r = 1/30, 1/10$, are chosen. From Fig. 3, the increase of rotational speed and hub radius gives rise to an increase of the natural frequencies. The reason is that both of them lead to the increase of a centrifugal force, as if the beams are stiffened. It is again viewed that the rotary inertia has a reductive effect on the natural frequencies. In particular, the fundamental frequency curve with $r_0 = 0$ and $r = 1/10$ intersects the line of the speed $\lambda = \eta$ at the position $\eta = 62.37$, which produces the tuned angular speed, and in this case resonance occurs. When the

fundamental frequencies are far away from the straight line $\lambda = \eta$, resonance phenomenon does not occur.

Fig. 4 depicts the first five dimensionless frequency curves as a function of the taper ratio c for a rotating Rayleigh beam with $r = 1/30$, $r_0 = 0, 0.5, 2$, $\eta = 5$. From Fig. 4, the natural frequencies except the fundamental ones decrease as the taper ratio increases. However, for the fundamental frequencies, the taper ratio leads to a slight increase, which can be observed from those listed in Tables 3 and 4. This means that the fundamental frequencies have a reverse trend of change as compared to other higher-order frequencies.

For three different rotational speeds $\eta = 0, 5$ and 10, Fig. 5 shows the first four dimensionless frequency increments $(\lambda_\eta - \lambda_{\eta=0})$ versus the dimensionless hub radius with $c = 0.5$, $r = 1/30$. For a non-rotating beam $(\eta = 0)$, the frequency has no increment since these curves are overlapped horizontal lines passing through the origin. This infers that the hub radius has no effect on the natural frequencies for a non-rotating beam. Nevertheless, for a rotating beam $(\eta \neq 0)$, the increasing of hub radius gives rise to a nearly linear increase of the natural frequencies.

Finally, considering or neglecting the effect of the $\rho I\Omega^2 \partial w/\partial x$ term, the percentage errors of the natural frequencies as a function of the rotational speed η are presented for the first two vibration modes with $r_0 = 0.5$, $c = 0, 0.25, 0.5$, $r = 1/30, 1/10$, in Figs. 6 and 7, respectively. Figs. 6 and 7 show that the errors increase as the rotational speeds are increased, it is due to the increasing effect of the $\rho I\Omega^2 \partial w/\partial x$ term resulting from the increase of rotational speed, as reported in [20], the effect of the $\rho I\Omega^2 \partial w/\partial x$ term on natural frequencies is remarkable for the high rotational speed particularly. Realistically, the $\rho I\Omega^2 \partial w/\partial x$ term have no effect on natural frequencies for a non-rotating beam with $\eta = 0$, and the error curves go through the origin all the time. It is also viewed that the increasing of rotary inertia directly leads to an increase of the error, similarly, it is because of the increasing effect of the $\rho I\Omega^2 \partial w/\partial x$ term resulting from the increase of rotary inertia. Besides, the error decreases as the taper ratio is increased, this is resulting from the decrease of the $\rho I\Omega^2 \partial w/\partial x$ term because of the weakened cross-sectional area and moment, as viewed in Eqs. (13) and (14). Moreover, as observed from Table 6, the error remains positive, and considering the $\rho I\Omega^2 \partial w/\partial x$ term gives rise to the decrease of natural frequencies.

5. Conclusions

The free vibration of rotating non-uniform Rayleigh cantilever beams was studied. The integral equation method was applied to determine numerical results of the natural frequencies. Since rotary inertia has been taken into account, the results are more practical than those using the Euler–Bernoulli beam theory. Numerical frequencies were presented for rotating tapered beams with typically varying cross-sections including linearly varying depth and/or width. Some conclusions are drawn as follows.

- Increasing rotary inertia has a decreasing effect on the natural frequencies.
- Increasing rotational speed has an increasing effect on the natural frequencies.
- Resonance occurs for rotating beams with high rotary inertia.
- Increasing taper ratio has a decreasing effect on the natural frequencies, but has a slightly increasing effect on the fundamental frequencies.
- Increasing hub radius has an increasing effect on the natural frequencies.
- Increasing the term, $\rho I\Omega^2 \partial w/\partial x$ has a decreasing effect on the natural frequencies, and the effect is remarkable for high rotational speed.

Acknowledgments

This work was supported by the Open Foundation of State Key Laboratory of Structural Analysis for Industrial Equipment, Dalian University of Technology, PR China (No. GZ1308), and the Faculty Research Foundation of Central South University, PR China (No. 2013JSJJ020).

References

[1] Gunda JB, Ganguli R. New rational interpolation functions for finite element analysis of rotating beams. Int J Mech Sci 2008;50:578–88.
[2] Vinod KG, Gopalakrishnan S, Ganguli R. Free vibration and wave propagation analysis of uniform and tapered rotating beams using spectrally formulated finite elements. Int J Solids Struct 2007;44:5875–93.
[3] Ozdemir O, Kaya MO. Flapwise bending vibration analysis of a rotating tapered cantilever Bernoulli–Euler beam by differential transform method. J Sound Vib 2006;289:413–20.
[4] Firouz-Abadi RD, Haddadpour H, Novinzadeh AB. An asymptotic solution to transverse free vibrations of variable-section beams. J Sound Vib 2007;304:530–40.
[5] Ozgumus OO, Kaya MO. Energy expressions and free vibration analysis of a rotating double tapered Timoshenko beam featuring bending–torsion coupling. Int J Eng Sci 2007;45:562–86.
[6] Banerjee J, Su H, Jackson D. Free vibration of rotating tapered beams using the dynamic stiffness method. J Sound Vib 2006;298:1034–54.
[7] Ganesh R, Ganguli R. Stiff string approximations in Rayleigh–Ritz method for rotating beams. Appl Math Comput 2013;219:9282–95.
[8] Ozgumus OO, Kaya MO. Flapwise bending vibration analysis of a rotating double-tapered Timoshenko beam. Arch Appl Mech 2008;78:379–92.
[9] Hodges DY, Rutkowski MY. Free-vibration analysis of rotating beams by a variable-order finite-element method. AIAA J 1981;19:1459–66.
[10] Wang G, Wereley NM. Free vibration analysis of rotating blades with uniform tapers. AIAA J 2004;42:2429–37.
[11] Yan S-X, Zhang Z-P, Wei D-J, Li X-F. Bending vibration of rotating tapered cantilevers by integral equation method. AIAA J 2011;49:872–6.
[12] Tsai MH, Lin WY, Zhou YC. Investigation on steady state deformation and free vibration of a rotating inclined Euler beam. Int J Mech Sci 2011;53:1050–68.
[13] Rao SS, Gupta RS. Finite element vibration analysis of rotating Timoshenko beams. J Sound Vib 2001;242:103–24.
[14] Ozgumus OO, Kaya MO. Energy expressions and free vibration analysis of a rotating Timoshenko beam featuring bending–bending-torsion coupling. Arch Appl Mech 2013;83:97–108.
[15] Yoo HH, Shin SH. Vibration analysis of rotating cantilever beams. J Sound Vib 1998;212:807–28.
[16] Chung J, Yoo HH. Dynamic analysis of a rotating cantilever beam by using the finite element method. J Sound Vib 2002;249:147–64.
[17] Chung J, Yoo HH. Dynamic analysis of a rotating cantilever beam by using the finite element method. J Sound Vib 2002;249:147–64.
[18] Huang CL, Lin WY, Hsiao KM. Free vibration analysis of rotating Euler beams at high angular velocity. Comput Struct 2010;88:991–1001.
[19] Al-Ansary MD. Flexural vibrations of rotating beams considering rotary inertia. Comput Struct 1998;69:321–8.
[20] Ozgumus OO, Kaya M. Vibration analysis of a rotating tapered Timoshenko beam using DTM. Meccanica 2010;45:33–42.
[21] Banerjee JR. Free vibration of centrifugally stiffened uniform and tapered beams using the dynamic stiffness method. J Sound Vib 2000;233:857–75.
[22] Banerjee JR, Jackson DR. Free vibration of a rotating tapered Rayleigh beam: a dynamic stiffness method of solution. Comput Struct 2013;124:11–20.
[23] Banerjee JR. Dynamic stiffness formulation and free vibration analysis of centrifugally stiffened Timoshenko beams. J Sound Vib 2001;247:97–115.
[24] Li XF, Tang AY, Xi LY. Vibration of a Rayleigh cantilever beam with axial force and tip mass. J Constr Steel Res 2013;80:15–22.
[25] Xi LY, Li XF, Tang GJ. Free vibration of standing and hanging gravity-loaded Rayleigh cantilevers. Int J Mech Sci 2013;66:233–8.
[26] Du H, Lim MK, Liew KM. A power series solution for vibration of a rotating Timoshenko beam. J Sound Vib 1994;175:505–23.
[27] Lee SY, Kuo YH. Bending frequency of a rotating Timoshenko beam with general elastically restrained root. J Sound Vib 1993;162:243–50.
[28] Kaya MO. Free vibration analysis of a rotating Timoshenko beam by differential transform method. Aircr Eng Aerosp Tec 2006;78:194–203.
[29] Rossi RE, Laura PaA, Maurizi MJ. Numerical experiments on the effect of the value of the shear coefficient upon the natural frequencies of a Timoshenko beam. J Sound Vib 1992;154:374–9.
[30] Paz M. Structural dynamics: theory and computation. Springer; 1997.